coatings

MDPI

Article

Synthesized TiO_2 Mesoporous by Addition of Acetylacetone and Graphene for Dye Sensitized Solar Cells

Chun-Hao Chang [1], Chia-Han Chuang [2], De-Yang Zhong [2], Jun-Cheng Lin [2], Chia-Chi Sung [1,*] and Chun-Yao Hsu [2,*]

[1] Department of Engineering Science and Ocean Engineering, National Taiwan University, Taipei 10617, Taiwan; a26818986@gmail.com
[2] Department of Mechanical Engineering, Lunghwa University of Science and Technology, Taoyuan 33306, Taiwan; g1082111004@gm.lhu.edu.tw (C.-H.C.); asdfzxcv0121@gmail.com (D.-Y.Z.); d1044142046@gm.lhu.edu.tw (J.-C.L.)
* Correspondence: ccsung@ntu.edu.tw (C.-C.S.); cyhsu@mail.lhu.edu.tw (C.-Y.H.); Fax: +886-6-82094845 (C.-Y.H.)

Abstract: This study mixed acetylacetone (Acac, 1, 2, and 3 mL) and graphene powder (GP, 0 wt.%, 0.001 wt.%, 0.003 wt.% and 0.005 wt.%) with TiO_2 mesoporous (TiO_2 powders: 20 g and particle size ~30 nm) to enhance the optoelectronic performances of dye sensitized solar cells (DSSC). Sponge-like structure TiO_2 mesoporous layers is a requirement for obtaining high efficiency DSSC, which ia synthesized by spin-coating techniques. The dense TiO_2 blocking layer (using peroxo-titanium complex) has a uniform, dense structure and completely adheres to the substrates to avoid charge recombination. The X-ray diffraction (XRD) and transmission electron microscopy (TEM) analyses of the TiO_2 films display the anatase type phase with preferred orientation along the (101) direction. After being ball milled, the TiO_2 mesoporous particle size almost remains unchanged. For mixing the Acac with TiO_2, the Raman intensity relatively increased, and the band gap energy (Eg) value decreased from 3.223 eV (for pure TiO_2) to 3.076 eV (for 2 mL Acac). Raman spectroscopy is used to evaluate the GP elements. It can be seen the intensity ratio (I_D/I_G) and (I_{2D}/I_G) was enhanced when the GP concentration increased. Using mixed Acac 2 mL and GP 0.003 wt.% with a TiO_2 mesoporous, led to increases in the open circuit voltage (V_{OC}), short circuit current density (J_{SC}) and fill factor (FF). If a fluorine-doped tin oxide is used instead of an indium tin oxide glass substrate, the photovoltaic efficiency of DSSC increases from 5.45% to 7.24%.

Keywords: DSSC; TiO_2 mesoporous; band gap; photovoltaic efficiency

Citation: Chang, C.-H.; Chuang, C.-H.; Zhong, D.-Y.; Lin, J.-C.; Sung, C.-C.; Hsu, C.-Y. Synthesized TiO_2 Mesoporous by Addition of Acetylacetone and Graphene for Dye Sensitized Solar Cells. *Coatings* **2021**, *11*, 796. https://doi.org/10.3390/coatings11070796

Academic Editors: Maria Vittoria Diamanti and Aivaras Kareiva

Received: 19 April 2021
Accepted: 29 June 2021
Published: 1 July 2021

1. Introduction

Dye-sensitized solar cells (DSSC) have attracted considerable attention as potential candidates for next-generation solar cells [1]. It is generally accepted that the low synthesis cost, simple structure, reasonable power conversion efficiency (in the range from 5% to 11% [2]), renewability, clean energy source [3,4], and ability to be used on flexible substrates makes them desirable [5]. DSSC is a photo-electrochemical processes system, consisting of three components [6]: (a) a working electrode, a transparent conducting glass covered with a porous TiO_2 semiconductor sensitized by the dye, (b) an iodide electrolyte, a liquid solution of redox mediator in the organic solvent and (c) a counter electrode, which generally uses Pt film as a catalyst [7,8]. A schematic diagram of the assembled DSSC is shown in Figure 1. Kouhestanian et al. [9] used ZnO nano-materials as a blocking layer on the transparent conducting glass, to inhibit the electron recombination reactions occurring with a traditional TiO_2-based DSSC. As a result, the ZnO-TiO_2 structures play a key role in DSSC performance, and optimum photovoltaic efficiency is obtained.

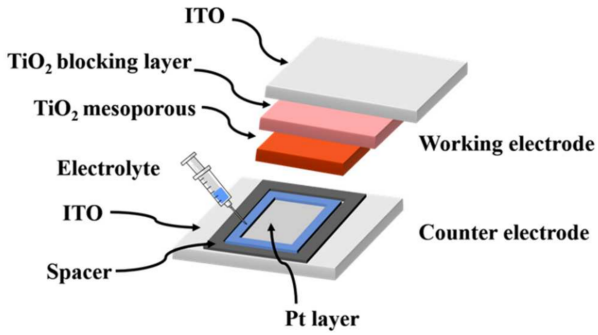

Figure 1. Schematic diagram of the assembled DSSC.

TiO_2 is found in many applications because of its commercial availability, low cost, robustness, long-term chemical stability, nontoxic nature, superior optoelectronic properties, beneficial charge carrier features and high transparency in the DSSC spectrum [10]. The spin coating technique offers simple ways to synthesize TiO_2 layers, with high control of the grain sizes, surface area, morphology and structure [11,12]. Umale et al. [13] synthesized TiO_2 nanocrystalline as an anodic material to examine the photovoltaic performance of DSSC. The improved performance was attributed to better charge transport and a much superior conversion efficiency was achieved. Udomrungkhajornchai et al. [14] reported the effects of adding a nonionic surfactant to TiO_2 to increase the optoelectronic features of DSSC, utilizing nontoxic electrolytes and natural sensitized-dye. A significant influence of the active cell size was confirmed. Further, using a proper amount of Triton X-100 could enhance the efficiency of DSSC. Kandasamy et al. [15] prepared aminosilicate modifying porous TiO_2 graphene oxide composite using hydrothermal techniques. The modified TiO_2 graphene materials have high surface area, demonstrating appropriate dye loading for light harvesting and offering good electrolyte connection. When decreasing the back-electron transfer between dye molecules and photo-anode, much higher photovoltaic efficiency (5.11%) than that of the unmodified porous TiO_2 (3.92%) is shown.

TiO_2 is a good photo-anode material in DSSC, causing greater specific surface area for adsorption of a high density of dye. However, it has high intrinsic band gap energy (about 3.2 eV) that can only absorb sunlight in the ultraviolet wavenumber region, resulting in low solar spectrum utilization [16]. To expand the solar energy absorption of TiO_2 to the visible region and promote electron transport, various dopants have been added to enhance photovoltaic efficiency [17]. This study synthesized Acetylacetone (Acac, liquids solution) and Graphene powder (GP, nano-particle 5–10 nm) mixed with TiO_2 mesoporous as photo-anodes in the DSSC by means of the spin-coating method. The influence of dopant contents on the crystal phase structure, surface morphology, optical band gap and DSSC performance were analyzed in detail.

2. Experimental Details

Prior to deposition of the film, the substrates were ultrasonically cleaned in a detergent bath, isopropyl alcohol and acetone, respectively, and then rinsed with deionized water, and blow-dried with nitrogen. The TiO_2 blocking layer was formed by the peroxo-titanium complex aqueous solution ($TiCl_4$, Sigma-Aldrich, St. Louis, MO, USA, 189.68). $TiCl_4$ (0.5 mL) was dissolved in deionized water (50 mL) at a temperature of 0–3 °C, and then with the addition of H_2O_2 (2 mL), stirred for 1 h at room temperature. The TiO_2 blocking layer was deposited by immersion of indium tin oxide (ITO)/glass substrates in the solution for 12 h. The TiO_2 blocking layer was rinsed with deionized water, dried and then sintered at 460 °C for 35 min in air.

The TiO_2 powders (20 g, average particle size ~30 nm, Anatase (80%), Rutile (20%)), deionized water (30 mL), Triton X-100 (0.5 mL), PEG-20000 (0.5 g), Acac and GP were mixed together, ball-milled for 7 days and then stirred for 24 h. The Acac (0, 1, 2 and 3 mL)- and GP (0 wt.%, 0.001 wt.%, 0.003 wt.%, and 0.005 wt.%)-mixed with TiO_2 mesoporous

were applied by spin-coating techniques onto a TiO_2 blocking layer. The thin films were sintered at 500 °C for 30 min in vacuum ambient (1.2 Pa), which transforms the crystal structure into an anatase phase and benefits DSSC performance. To sensitize the TiO_2 mesoporous electrodes, they were submerged in anhydrous ethanol containing 0.5 mM N719 ($C_{58}H_{86}N_8O_8RuS_2$) dye for 24 h in a dark box at room temperature. The specimens were washed with acetone to remove extra unanchored dye molecules. The Pt (50 nm thick) counter electrode was coated onto another ITO/glass substrate by sputtering with pure Ar plasma gas and a direct current power of 40 watts. Two different types of electrode (TiO_2 working electrode with the absorbed dye and Pt counter electrode) were assembled together to form a cell. The electrolyte solution (Iodolyte HI-30, Solaronix, Aubonne, Switzerland) was injected into the cell. Table 1 lists the chemical abstract service (CAS) numbers of all the chemical elements and substrates.

Table 1. Chemical abstracts service (CAS) numbers of all the chemical elements and substrates.

TiCl4	7550-45-0
TiO2	13463-67-7
Triton™ X-100	9002-93-1
Polyethylene Glycol 20,000	25322-68-3
H2O2	7722-84-1
N719	207347-46-4
Electrolyte Solution (Iodolyte HI-30)	75-05-8
Graphene Powder	1034343-98-0
Acetylacetone	123-54-6
Indium Tin Oxide (ITO)	50926-11-9
Soda Lime Glass	8006-28-8

The film specimens were characterized for the phase structure using an X-ray diffractometer (XRD, BRUKER, D8 DISCOVER SSS Multi Function High Power X-ray, Tokyo, Japan) utilizing Cu-Kα radiation, a grazing incidence angle of 1° and a scanning rate of 2°/min. The morphology of the film was examined using a field emission scanning electron microscope (JEOL JSM-6500F, SEM, Zeiss, Germany). The nanostructure of the films was characterized using a transmission electron microscope (Philips Tecnai F20 G2 FEI-TEM, Tokyo, Japan). The particle grain size using a laser scattering particle size distribution analyzer (HORIBA LA-950, Kyoto, Japan). The thickness of the film was estimated by a surface profilometer (α-step, ET-4000A KOSAK, Taipei, Taiwan). The optical transmittance spectra were examined with a UV–vis spectrophotometer (Jasco V-655, Tokyo, Japan). The structure of the film was characterized by Raman scattering spectroscopy (iHR550, Horiba, France). The photovoltaic conversion efficiency was evaluated using the current–voltage (J–V) features of DSSC. The J–V characteristic curves for the DSSC devices were determined by a solar simulator (150 W simulator, Bunko-Keiki Co. Ltd., Munich, Germany) with a Xenon Lamp light source (AM 1.5 spectrum, irradiance of 100 mW/cm^2, Tokyo, Japan). To ensure the reproducibility of the results, all tests were measured four times and average values are cited.

3. Results and Discussion

Setting a dense blocking layer (compact layer) between the transparent conductive oxide and the TiO_2 mesoporous to prevent the electron/hole recombination at the conducting oxide/electrolyte interface, results in higher photocurrents density and open-circuit photovoltages [18,19]. Figure 2 shows the SEM images of the thin TiO_2 blocking layer (using peroxo-titanium complex) coated on ITO/glass. The surface of the sample was flat and some irregular nodule particles of around 50 nm in size appeared, randomly distributed on the surface. The TiO_2 blocking layer is about 20 nm thick, with a uniform and dense structure, no micro-cracks and completely adhering to the ITO/glass. Figure 3 shows the X-ray diffraction patterns of the TiO_2 blocking layer and bare ITO. It can be seen the predominant orientations of the bare ITO films are the (222) and (400) diffraction

peak. A similar characteristic was obtained by Gheidari et al. [20]. Modifying the surface of the ITO/glass with a TiO_2 blocking layer, the diffraction peak for anatase (101) TiO_2 was observed at ~37.7° (JCPDS pattern No. 21-1272).

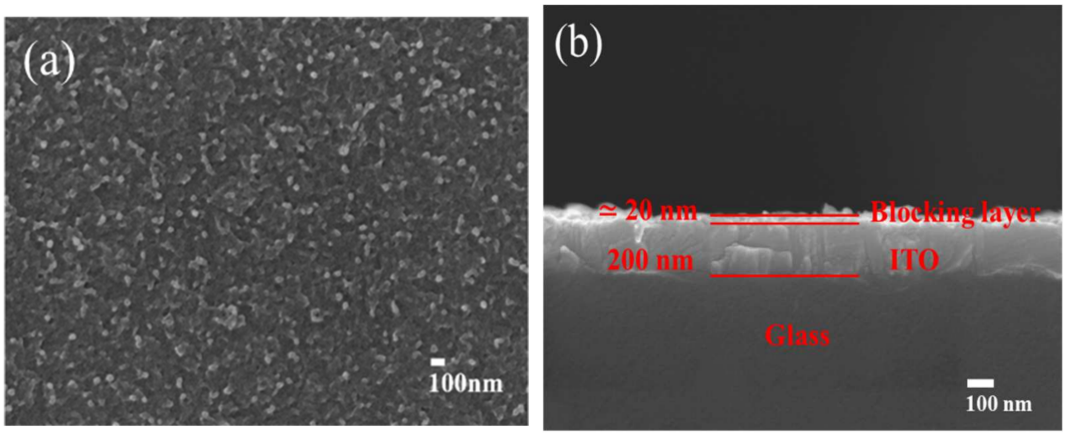

Figure 2. SEM images of the TiO_2 blocking layer coated on ITO/glass (**a**) plan-view (**b**) cross-section.

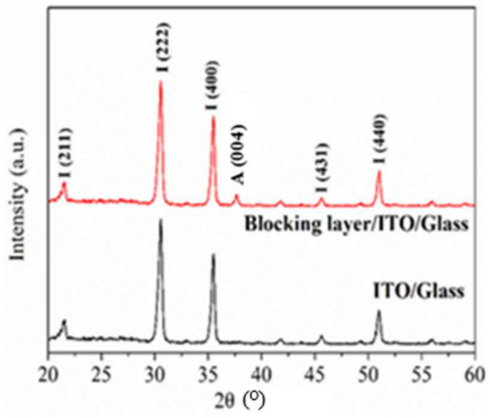

Figure 3. X-ray diffraction patterns of the TiO_2 blocking layer coated on ITO/glass and bare ITO.

The SEM and laser scattering images for particle size of TiO_2 powders with and without the ball milled sample, are shown in Figure 4. Without being ball milled (Figure 4a,b), it can be seen that particles severely agglomerated and particle size is about 33.7 nm. After being ball milled (Figure 4c,d), the TiO_2 particle size almost remains unchanged, and is shown dispersed homogeneously and without aggregations. Figure 5 shows an SEM cross-sectional morphology for the TiO_2 mesoporous coated on the TiO_2 blocking layer/ITO/glass by the sol–gel method. No cracking or peeling is observed following deposition. The TiO_2 mesoporous confirmed a sponge like structure, which is a requirement for obtaining high efficiency DSSC [21].

3.1. Mixed Acac with TiO_2 Mesoporous

Figure 6 shows the image of pure TiO_2 and mixed Acac with TiO_2 mesoporous following a sintering process at 500 °C for 30 min in an ambient vacuum (1.2 Pa). Figure 6a pure TiO_2 shows the agglomerated particles with a flake shape are embedded. The SEM images (Figure 6b–d) show the mixed Acac (1, 2, and 3 mL) with TiO_2 nanoparticles exhibiting near-spherical morphology and agglomeration. Figure 7a shows the X-ray diffraction spectrum in the 2θ range 20°–60°, for mixed Acac (0, 1, 2, and 3 mL) with a TiO_2 mesoporous layer (corresponding to Figure 6). All specimens show well consistent with crystalline TiO_2 anatase phase, representing that modified with Acac are suitable for the synthesis of crystalline TiO_2. For the mixed Acac with a TiO_2 mesoporous sample, the

rutile (110) phase disappeared and the other crystal phase was not detected. However, there was a slight decrease in the intensity of the main diffraction (101) peak after mixing. Figure 7b shows the TEM images with the selected-area electron diffraction (SAED) pattern of the TiO_2 layer. The diffraction rings in correspond well with (101) and (200) planes of anatase TiO_2. The (101) crystal structure of anatase had lower surface energy and was expected to be more stable than the other planes [21].

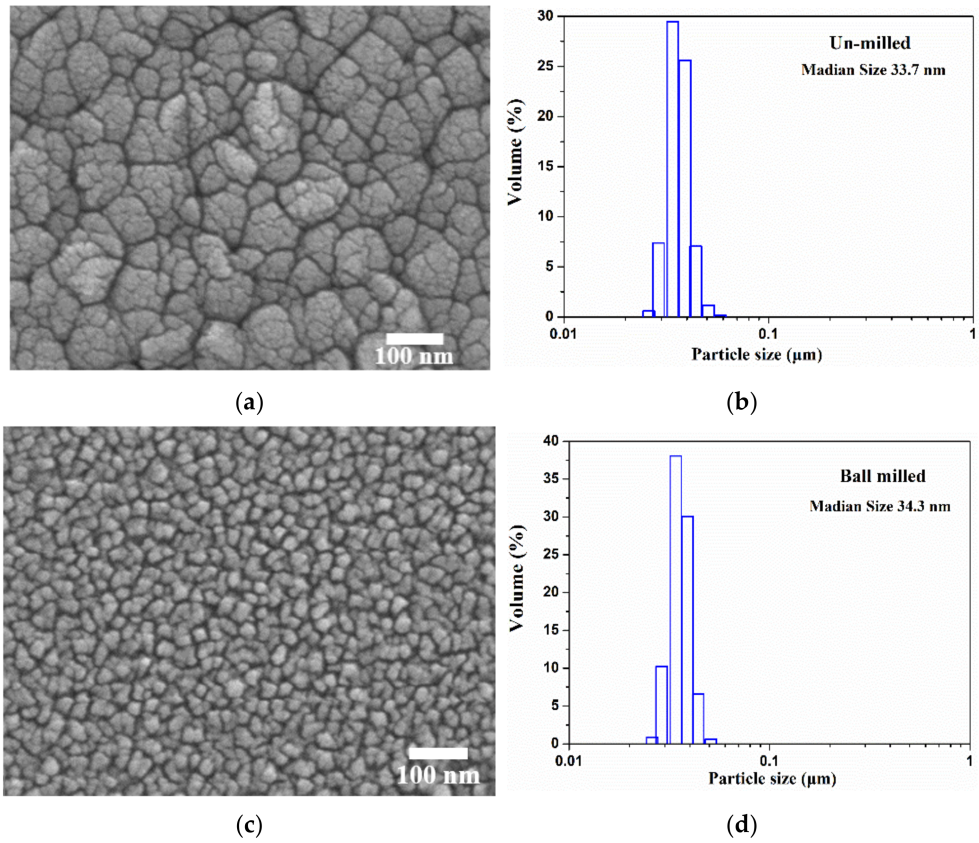

Figure 4. SEM (left) and laser scattering (right) images for particle size of TiO_2 powders: (**a**,**b**) un-milled and (**c**,**d**) ball milled samples.

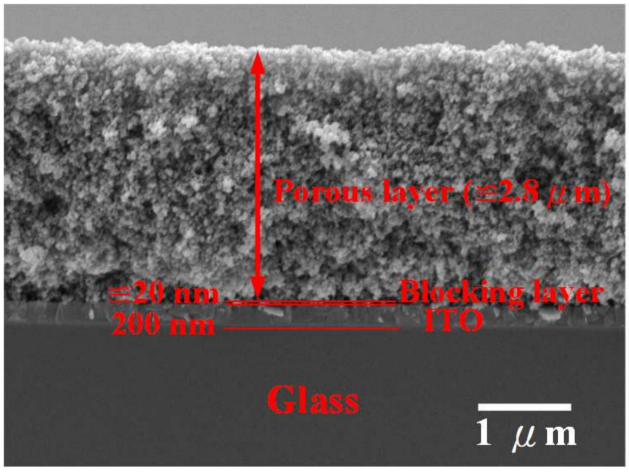

Figure 5. SEM cross-sectional image of the TiO_2 mesoporous coated on TiO_2 blocking layer/ITO/glass by the sol–gel method.

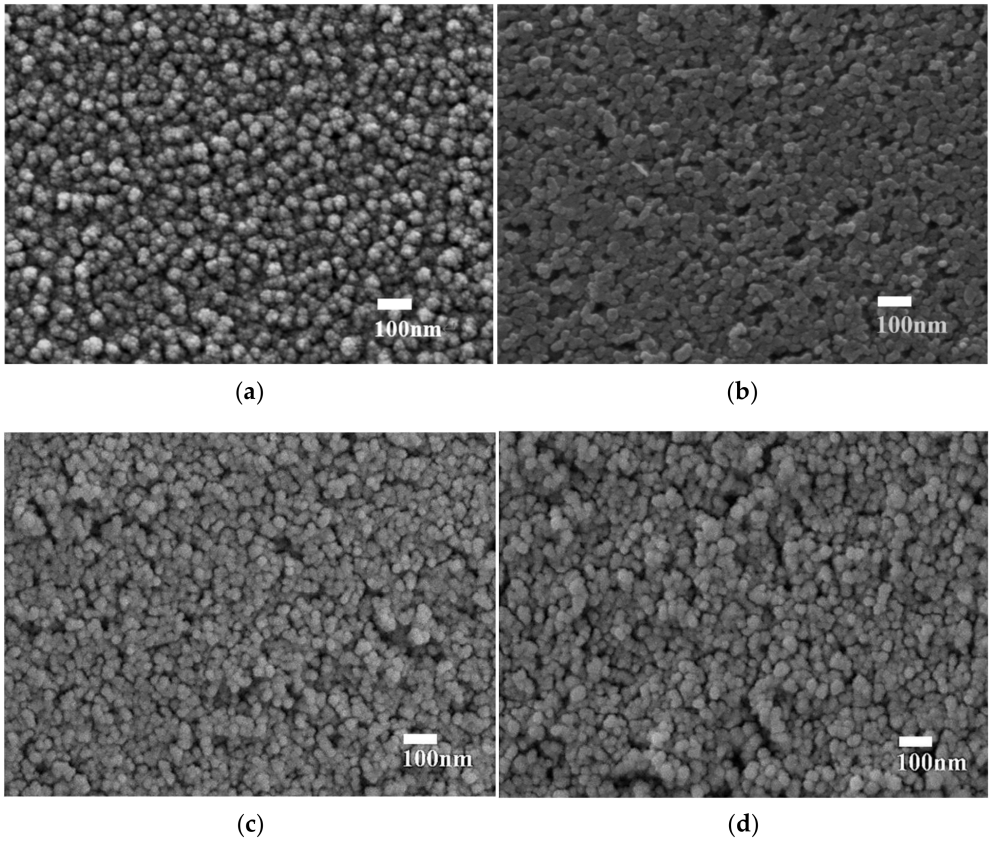

Figure 6. SEM photographs of the mixed Acac (0–3 mL) with a TiO_2 mesoporous layer. (**a**) Acac 0 mL TiO_2 mesoporous, (**b**) Acac 1 mL TiO_2 mesoporous, (**c**) Acac 2 mL TiO_2 mesoporous, (**d**) Acac 3 mL TiO_2 mesoporous.

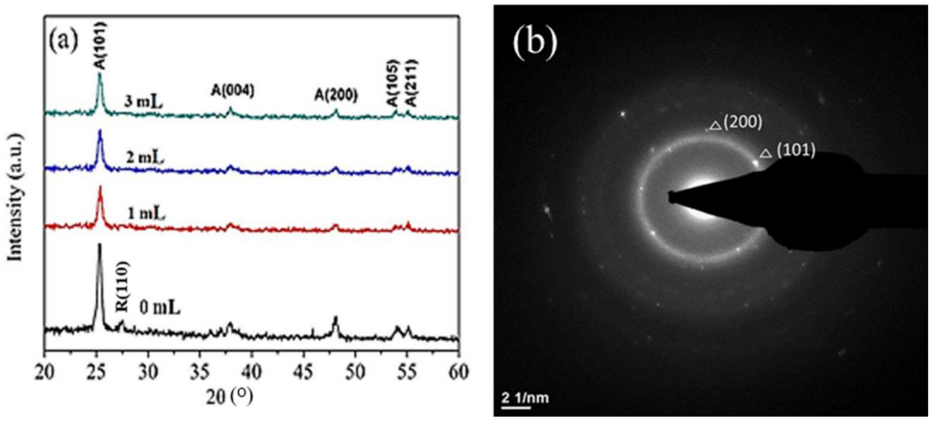

Figure 7. X-ray diffraction spectrum for (**a**) the mixed Acac (0, 1, 2, and 3 mL) with a TiO_2 mesoporous layer (**b**) TEM image of the TiO_2 film.

Figure 8 shows the Raman spectra for the mixed Acac (0, 1, 2, and 3 mL) with a TiO_2 mesoporous layer. Raman modes can be assigned to the Raman spectra of the anatase structure: ~148 (E_g), 198 (E_g), 398 (B_{1g}), 523 (A_{1g}), 524 (B_{1g}) and 642 cm^{-1} (E_g), which are typical of the D_{2d} point group and indicate the anatase phase [22]. For mixing the Acac with TiO_2, the Raman intensity relatively increased, which can be considered a surface-modified TiO_2 mesoporous by Acac. These results are consistent with those of the reported by Menezes et al. [22].

The TiO_2 optical characteristics rely on the ionic radius of the dopant elements and the chemical properties of the dopants [23]. Mixed non-metal elements with TiO_2 changes the energy states in the band gap, affecting the sunlight absorbance region and the electron

transport of the TiO_2 [24]. Figure 9 shows the band gap energy (Eg) as a function of mixing the Acac (0, 1, 2, and 3 mL) with a TiO_2 mesoporous layer. For mixing the Acac with TiO_2, the Eg value decreased to 3.181 eV (for 1 mL Acac) and 3.076 eV (for 2 mL Acac), respectively. The Eg of pure TiO_2 is 3.223 eV, the transition from the valence band to conduction band, which attributes to the charge transfer transition from O^{2-} to Ti^{4+}. This value is in agreement with the TiO_2 anatase particles. For the mixing the Acac with TiO_2 sample, a lower Eg is 3.076 eV. However, the Eg increased to 3.374 eV with the increased Acac concentration. All specimens were very close to the studied Eg value of the anatase structure [23].

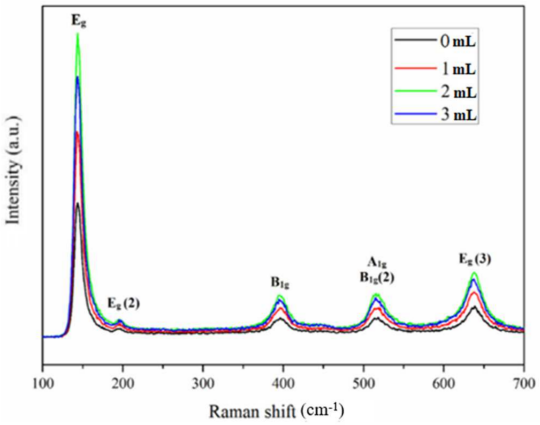

Figure 8. Raman spectra for for the mixed Acac (0, 1, 2, and 3 mL) with a TiO_2 mesoporous layer, corresponding to Figure 6.

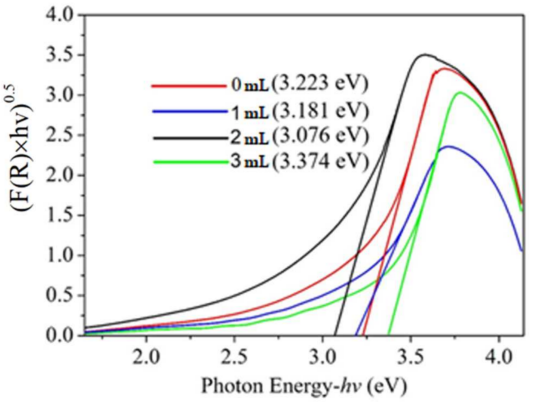

Figure 9. Band gap energy for the mixed Acac (0, 1, 2, and 3 mL) with a TiO_2 mesoporous layer, corresponding to Figure 6.

The current–voltage characteristics of the DSSC photovoltaic efficiency, mixing the Acac (0, 1, 2, and 3 mL) with a TiO_2 mesoporous layer, are shown in Figure 10 and Table 2. The photovoltaic efficiency (η) ranges between 1.93% and 2.99%. The open circuit voltage (V_{OC}) increases from 0.537 to 0.580 V (the increase in the mixed Acac with TiO_2). The higher fill factor (FF) is about 59.6% and the higher short circuit current density (J_{SC}) is about 10.262 mA/cm^2 with the Eg value decreasing to 3.076 eV (for 2 mL Acac).

3.2. Mixed Acac and GP with TiO_2 Mesoporous

Figure 11 shows the SEM photographs of the mixed Acac and GP with a TiO_2 mesoporous layer. It is apparent the surface nano-structures of the TiO_2 mesoporous films differ from one another. Figure 11a shows mixed (Acec 2 mL + GP 0.001 wt.%) with TiO_2, which possess uniform surface coverage and a near-spherical shape structure due to low graphene contents and grain characteristics similar to Figure 6c. From Figure 11b,c, an

obvious dense structure and a small grain size and raised surface area is observed when the GP concentration increased, a beneficial effect of the photovoltaic efficiency of DSSC. Kazmi et al. [25] reported graphene-TiO_2 composites to examine the DSSC performance. It is seen the band gap energy and grain size of the synthesized composites were reduced, enhancing the DSSC properties. Mehmood et al. [26] synthesized DSSC with the graphene-TiO_2 as a photo-anode, offering a beneficial pathway for the transfer of electrons to the external circuit, improving the current density and promoting the photovoltaic characteristics of DSSC. This advantage of GP incorporation enhances charge transfer and electron collection, which results in decreased charge trapping and recombination that can occur at the surface of TiO_2.

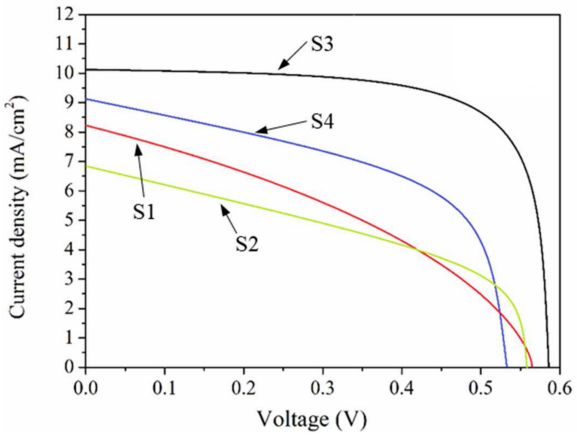

Figure 10. Current–voltage characteristics of the DSSC photovoltaic efficiency for mixed Acac (0, 1, 2, and 3 mL) with a TiO_2 mesoporous layer.

Table 2. The DSSC photovoltaic efficiency of mixed Acac (0–3 mL) with a TiO_2 mesoporous layer.

Device	V_{OC} (V)	J_{SC} (mA/cm^2)	FF (%)	η (%)
S1: pure TiO_2 layer	0.574 ± 0.005	8.18 ± 0.4	59.6 ± 1.2	2.79 ± 0.03
S2: mixed Acac 1 mL with TiO_2 layer	0.568 ± 0.004	6.76 ± 0.6	50.4 ± 1.0	1.93 ± 0.01
S3: mixed Acac 2 mL with TiO_2 layer	0.580 ± 0.004	10.26 ± 0.7	50.3 ± 1.3	2.99 ± 0.04
S4: mixed Acac 3 mL with TiO_2 layer	0.537 ± 0.003	9.16 ± 0.4	49.5 ± 1.1	2.43 ± 0.02

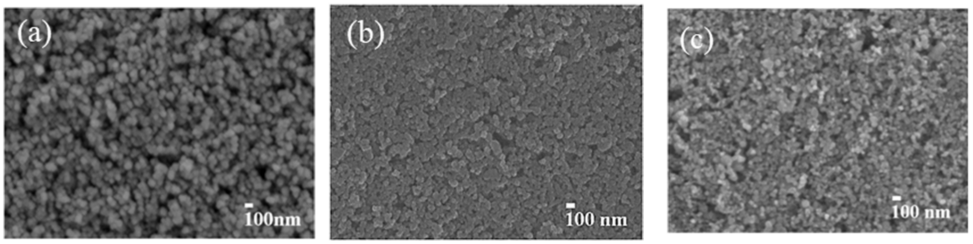

Figure 11. SEM photographs of the mixed Acac and GP with a TiO_2 mesoporous layer: (**a**) Acac 2 mL + GP 0.001 wt.%, (**b**) Acac 2 mL + GP 0.003 wt.% and (**c**) Acac 2 mL + GP 0.005 wt.%.

Raman spectroscopy is used to evaluate the carbon atomic bonding features [27]. The D-peak (disorder, 1310–1360 cm^{-1}) and G-peak (graphite, 1540–1580 cm^{-1}) for mixed Acac and GP with a TiO_2 mesoporous layer are shown in Figure 12. Table 3 lists the I_D/I_G ratio, I_{2D}/I_G and the position of the D-band and G-peak for mixed Acac and GP with a TiO_2 mesoporous layer. As can be seen, the intensity ratio (I_D/I_G) and (I_{2D}/I_G) grew when the GP concentration increased. Figure 13 shows the Eg for the mixed Acac (1, 2, and 3 mL) and GP (0 wt.%, 0.001 wt.%, 0.003 wt.% and 0.005 wt.%) with TiO_2 mesoporous layer. All samples were very near to the reported Eg value (~3.223 eV) of the anatase structure.

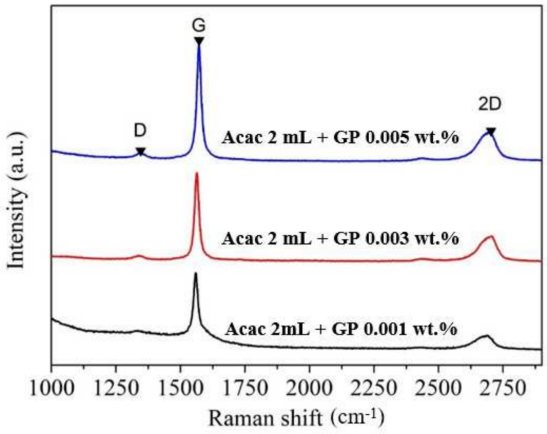

Figure 12. Raman spectra for the mixed Acac and GP with a TiO_2 mesoporous layer, corresponding to Figure 11.

Table 3. The I_D/I_G ratio, I_{2D}/I_G and the position of the D-band and G-peak for the mixed Acac and GP with a TiO_2 mesoporous layer.

Sample	D-Band	G-Band	2D-Band	I_D/I_G	I_{2D}/I_G
Acac 2 mL + GP 0.001 wt.%	1336.67	1560.21	2693.71	0.25	0.19
Acac 2 mL + GP 0.003 wt.%	1340.75	1564.18	2705.82	0.53	0.64
Acac 2 mL + GP 0.005 wt.%	1344.82	1572.13	2698.92	0.64	0.71

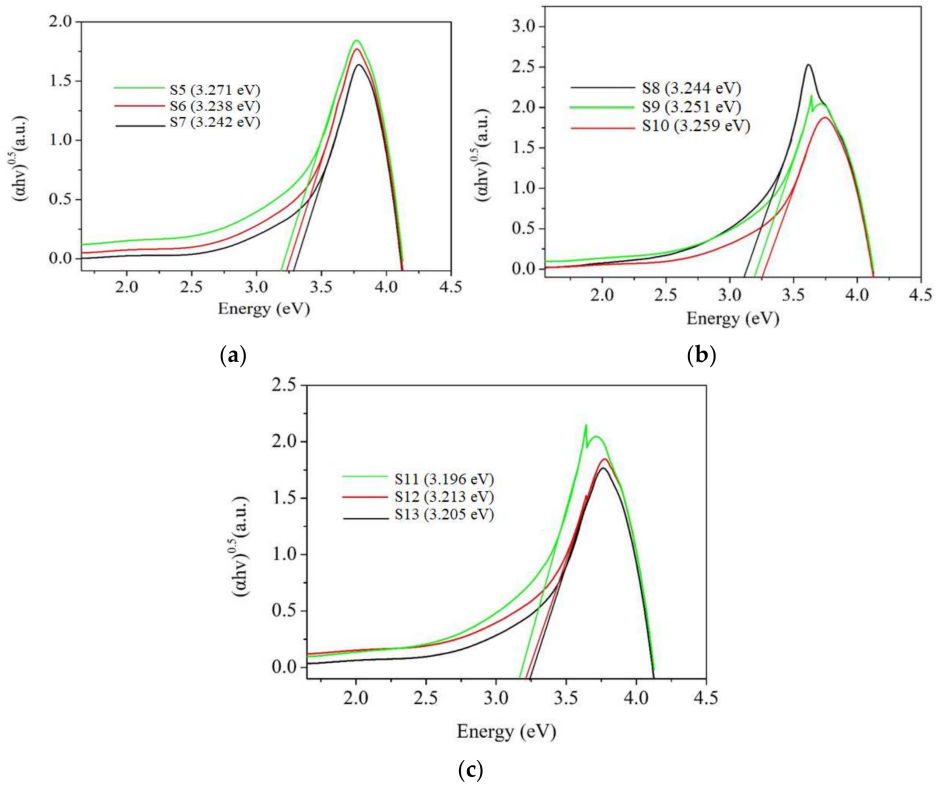

Figure 13. Band gap energy for mixed Acac and GP with a TiO_2 mesoporous layer. (**a**) fixed Acac 1 mL, various GP contents (S5: GP 0.001 wt.%, S6: GP 0.003 wt.%, S7: GP 0.005 wt.%); (**b**) fixed Acac 2 mL, various GP contents (S8: GP 0.001 wt.%, S9: GP 0.003 wt.%, S10: GP 0.005 wt.%); (**c**) fixed Acac 3 mL, various GP contents (S11: GP 0.001 wt.%, S12: GP 0.003 wt.%, S13: GP 0.005 wt.%).

Figure 14 shows the current–voltage characteristics of the DSSC photovoltaic efficiency, for the mixed Acac and GP with a TiO_2 mesoporous layer. As can be seen, the photovoltaic

efficiency increased when the GP element was mixed. The photovoltaic efficiency (η) ranges between 2.50% (for S11) and 5.45% (for the S9, mixed Acac 2 mL, GP 0.003 wt.% with a TiO_2 mesoporous layer). An increased V_{OC} value is caused by a proper amount of graphene (0.003 wt.%), with a higher conduction band level in the mixed GP with TiO_2 photoanodes compared to the case of pure TiO_2. This agrees with the consequences of Imbrogno et al. [28]. Higher J_{SC} is about 20.22 for the use of GP 0.005 wt.%. Promotion of the J_{SC} value usually concerns an increased number of photo-generated electrons that are efficiently transferred to the TiO_2 photoanodes [29]. This increased photovoltaic efficiency is attributed to smaller grain size, higher surface area and the promotion of dye adsorption.

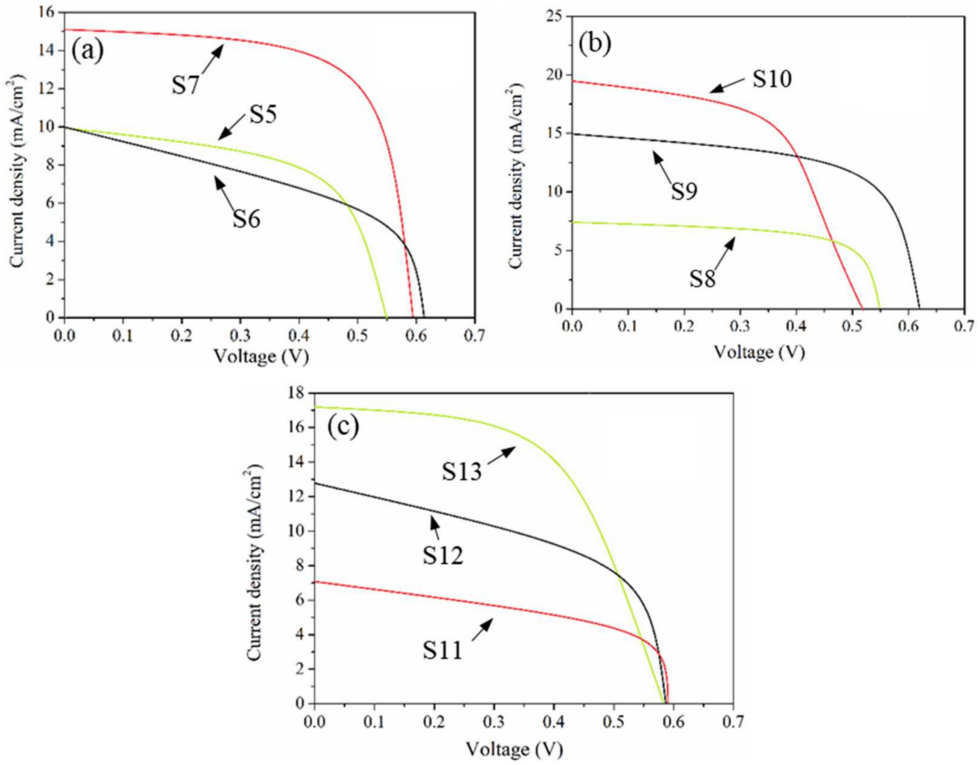

Figure 14. Current–voltage characteristics of the DSSC photovoltaic efficiency of the mixed Acac. and GP with a TiO_2 mesoporous layer, corresponding to Figure 13. (**a**) Fixed Acac 1 mL, various GP contents (S5: GP 0.001 wt.%, S6: GP 0.003 wt.%, S7: GP 0.005 wt.%); (**b**) fixed Acac 2 mL, various GP contents (S8: GP 0.001 wt.%, S9: GP 0.003 wt.%, S10: GP 0.005 wt.%); (**c**) fixed Acac 3 mL, various GP contents (S11: GP 0.001 wt.%, S12: GP 0.003 wt.%, S13: GP 0.005 wt.%).

3.3. Replace the ITO with Fluorine-Mixed Tin Oxide (FTO)/Glass

Due to the high temperature sintered (500 °C), the resistivity of ITO worsened (increasing from 20 to 100 Ω/sq), and the resistivity of FTO (20 Ω/sq) remained unchanged. The current–voltage characteristics of the DSSC photovoltaic efficiency, replacing the ITO with FTO/glass, are shown in Figure 15 and Table 4. Comparing S9 (mixed Acac 2 mL, GP 0.003 wt.% with TiO_2 porous) with S3 (mixed Acac 2 mL with TiO_2 porous), S9 shows the V_{OC} increases from 0.580 to 0.619 V, the J_{SC} increases from 10.26 to 14.81 mA/cm^2 and the FF increases from 50.3% to 59.5%. This could be due to the mixed GP with TiO_2 mesoporous leading to a higher conduction band level and raised surface area, promoting the photovoltaic efficiency of DSSC. Replacing the ITO (S9) with FTO (S14, mixed Acac 2 mL, GP 0.003 wt.% with a TiO_2 porous/Blocking layer/FTO) may significantly improve the number of electrons transferred from the photo-anodes to the counter electrode, leading to the J_{SC} increase from 14.81 to 21.65 mA/cm^2, and the increased photovoltaic efficiency of the DSSC from 5.45% to 7.24%.

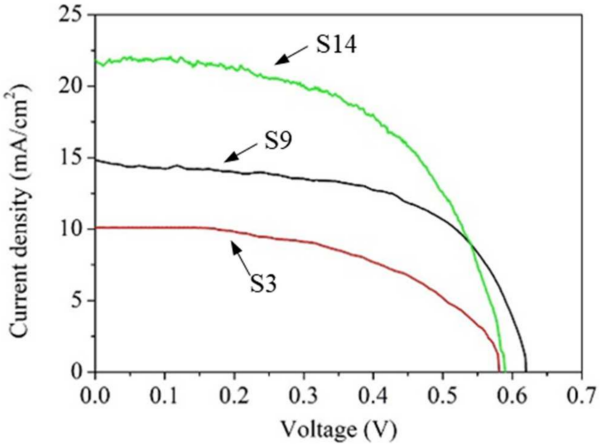

Figure 15. Current–voltage characteristics of the DSSC photovoltaic efficiency, replace the ITO with FTO/glass.

Table 4. DSSC photovoltaic efficiency, replacing the ITO with FTO/glass.

S3: Mixed Acac 2 mL with TiO_2 Porous/Blocking Layer/ITO **S9: Mixed Acac 2 mL and GP 0.003 wt.% with TiO_2 Porous/Blocking Layer/ITO** **S14: Mixed Acac 2 mL and GP 0.003 wt.% with TiO_2 Porous/Blocking Layer/FTO**				
–	**V_{oc} (V)**	**J_{sc} (mA/cm^2)**	**Fill Factor (%)**	**Eff. η (%)**
S3	0.580 ± 0.006	10.26 ± 0.7	50.3 ± 1.3	2.99 ± 0.02
S9	0.619 ± 0.008	14.81 ± 0.4	59.5 ± 1.1	5.45 ± 0.04
S14	0.593 ± 0.005	21.65 ± 0.6	56.4 ± 1.1	7.24 ± 0.07

4. Conclusions

This study synthesized mixed Acec (0, 1, 2, and 3 mL) and GP (0 wt.%, 0.001 wt.%, 0.003 wt.%, and 0.005 wt.%) with TiO_2 mesoporous on a TiO_2 blocking layer (thickness of 20 nm) as photo-anodes in the DSSC using the spin-coating method. All specimens show the anatase type phase of TiO_2. Mixed Acac and GP with a TiO_2 mesoporous sample did not detect the other crystal phase, and also did not change the TiO_2 crystalline structure. Comparing (mixed Acac 2 mL, GP 0.003 wt.%) with (mixed Acac 2 mL only) shows the V_{OC}, J_{SC}, and FF increase from 0.580 to 0.619 V, from 10.26 to 14.81 mA/cm^2 and from 50.3% to 59.5%, respectively. This could be due to the mixed GP with TiO_2 mesoporous leading to a higher conduction band level, smaller grain size, higher surface area and the promotion of dye adsorption, increasing the photovoltaic efficiency of DSSC.

After high temperature sintered (500 °C), the sheet resistance of ITO and FTO are 100 and 20 Ω/sq, respectively. Replacing the ITO with FTO may significantly improve the number of electrons transferred from the photoanode to the counter electrode, leading to J_{SC} increases from 14.81 to 21.65 mA/cm^2. The results show the photovoltaic efficiency of DSSC increased from 5.45% to 7.24%. In the confirmation runs, mixing Acac and GP with TiO_2 mesoporous is an easy and cheap process, which improved the photovoltaic efficiency and is beneficial to the DSSC academic development.

Author Contributions: Conceptualization, C.-H.C. (Chun-Hao Chang) and C.-H.C. (Chia-Han Chuang); methodology, D.-Y.Z.; software, D.-Y.Z.; validation, J.-C.L., C.-C.S., and C.-Y.H.; formal analysis, C.-H.C. (Chun-Hao Chang); investigation, C.-Y.H.; resources, C.-H.C. (Chun-Hao Chang); data curation, C.-H.C. (Chun-Hao Chang); writing—original draft preparation, C.-C.S.; writing—review and editing, C.-C.S.; visualization, D.-Y.Z.; supervision, J.-C.L.; project administration, C.-Y.H.; funding acquisition, C.-C.S. All authors have read and agreed to the published version of the manuscript.

Funding: Ministry of Science and Technology of the Republic of China, through Grant nos. MOST 109-2221-E-002-039.

Institutional Review Board Statement: Not applicable.

Informed Consent Statement: Not applicable.

Data Availability Statement: Not applicable.

Conflicts of Interest: No potential conflict of interest was reported by the authors.

References

1. Cheema, H.; Watson, J.; Delcamp, J.H. Photon management strategies in SSM-DSCs: Realization of a >11% PCE device with a 2.3 V output. *Sol. Energy* **2020**, *208*, 747–752. [CrossRef]
2. Xi, J.-Y.; Jia, R.; Li, W.; Wang, J.; Bai, F.-Q.; Eglitis, R.; Zhang, H.-X. How does graphene enhance the photoelectric conversion efficiency of dye sensitized solar cells? An insight from a theoretical perspective. *J. Mater. Chem. A* **2019**, *7*, 2730–2740. [CrossRef]
3. Mandal, S.; Kandregula, G.R.; Tokala, V.N.B. A computational investigation of the influence of acceptor moieties on photovoltaic performances and adsorption onto the TiO_2 surface in triphenylamine-based dyes for DSSC application. *J. Photochem. Photobiol. A Chem.* **2020**, *401*, 112745–112754. [CrossRef]
4. Tan, L.; Ong, W.; Chai, S.; Mohamed, A. Reduced graphene oxide-TiO_2 nanocomposite as a promising visible-light-active photocatalyst for the conversion of carbon dioxide. *Nanoscale Res. Lett.* **2013**, *8*, 1–8. [CrossRef]
5. Su, R.; Ashraf, S.; Lyu, L.; El-Shafei, A. Tailoring dual-channel anchorable organic sensitizers with indolo [2,3-b] quinoxaline moieties: Correlation between structure and DSSC performance. *Sol. Energy* **2020**, *206*, 443–454. [CrossRef]
6. Zalas, M.; Jelak, K. Optimization of platinum precursor concentration for new, fast and simple fabrication method of counter electrode for DSSC application. *Optik* **2020**, *206*, 164314–164319. [CrossRef]
7. Umar, M.I.A.; Haris, V.; Umar, A.A. The influence of $MoSe_2$ coated onto Pt film to DSSC performance with the structure TiO_2/Dye/L_xMoSe_2Pt ($0 \leq x \leq 5$). *Mater. Lett.* **2020**, *275*, 128076–128080. [CrossRef]
8. Zhang, L.; Cole, J.M. Anchoring groups for dye-sensitized solar cells. *ACS Appl. Mater. Interfaces* **2015**, *7*, 3427–3455. [CrossRef]
9. Kouhestanian, E.; Mozaffari, S.A.; Ranjbar, M.; Amoli, H.S. Enhancing the electron transfer process of TiO_2-based DSSC using DC magnetron sputtered ZnO as an efficient alternative for blocking layer. *Org. Electron.* **2020**, *86*, 105915–105927. [CrossRef]
10. Kumar, T.R.N.; Yuvaraj, S.; Kavitha, P.; Sudhakar, V.; Krishnamoorthy, K.; Neppolian, B. Aromatic amine passivated TiO_2 for dye-sensitized solar cells (DSSC) with ~9.8% efficiency. *Sol. Energy* **2020**, *201*, 965–971. [CrossRef]
11. Dubey, R.; Krishnamurthy, K.V.; Singh, S. Experimental studies of TiO_2 nanoparticles synthesized by sol-gel and solvothermal routes for DSSCs application. *Results Phys.* **2019**, *14*, 102390. [CrossRef]
12. Das, A.; Wary, R.R.; Nair, R.G. Cu modified ZnO nanoflakes: An efficient visible light-driven photocatalyst and a promising photoanode for dye sensitized solar cell (DSSC). *Solid State Sci.* **2020**, *104*, 106290. [CrossRef]
13. Umale, S.; Sudhakar, V.; Sontakke, S.M.; Krishnamoorthy, K.; Pandit, A.B. Improved efficiency of DSSC using combustion synthesized TiO_2. *Mater. Res. Bull.* **2019**, *109*, 222–226. [CrossRef]
14. Udomrungkhajornchai, S.; Junger, I.J.; Ehrmann, A. Optimization of the TiO_2 layer in DSSCs by a nonionic surfactant. *Optik* **2020**, *203*, 163945. [CrossRef]
15. Kandasamy, M.; Murugesan, S. Aminosilicate modified mesoporous anatase TiO_2@graphene oxide nanocomposite for dye-sensitized solar cells. *Sol. Energy* **2020**, *211*, 789–798. [CrossRef]
16. Ünlü, B.; Özacar, M. Effect of Cu and Mn amounts mixed to TiO_2 on the performance of DSSCs. *Sol. Energy* **2020**, *196*, 448–456. [CrossRef]
17. Ganesh, R.S.; Mamajiwala, A.Y.; Durgadevi, E.; Navaneethan, M.; Ponnusamy, S.; Muthamizhchelvan, C.; Shimura, Y.; Hayakawa, Y. Zn and Sr mixed TiO_2 mesoporous nanospheres as photoanodes in dye sensitized solar cell. *Mater. Chem. Phys.* **2019**, *234*, 259–267. [CrossRef]
18. Zatirostami, A. Increasing the efficiency of TiO_2-based DSSC by means of a double layer RF-sputtered thin film blocking layer. *Optik* **2020**, *207*, 164419. [CrossRef]
19. Huang, C.; Chang, K.; Hsu, C. TiO_2 compact layers prepared for high performance dye-sensitized solar cells. *Electrochim. Acta* **2015**, *170*, 256–262. [CrossRef]
20. Gheidari, A.M.; Soleimani, E.A.; Mansorhoseini, M.; Mohajerzadeh, S.; Madani, N.; Shams-Kolahi, W. Structural properties of indium tin oxide thin films prepared for application in solar cells. *Mater. Res. Bull.* **2005**, *40*, 1303–1307. [CrossRef]
21. Hočevar, M.; Krašovec, U.O.; Bokalič, M.; Topič, M.; Veurman, W.; Brandt, H.; Hinsch, A. Sol-gel based TiO_2 paste applied in screen-printed dye-sensitized solar cells and modules. *J. Ind. Eng. Chem.* **2013**, *19*, 1464–1469. [CrossRef]
22. Menezes, B.; Moreira, D.; Oliveira, H.; Marques, L.; Lima, J. Solvothermal synthesis of cerium-doped titania nanostructured materials modified with acetylacetone for solar-driven photocatalysis. *J. Braz. Chem. Soc.* **2020**, *31*, 153–161. [CrossRef]
23. Pal, M.; Pal, U.; Jiménez, J.M.G.Y.; Pérez-Rodríguez, F. Effects of crystallization and dopant concentration on the emission behavior of TiO_2: Eu nanophosphors. *Nanoscale Res. Lett.* **2012**, *7*, 1–12. [CrossRef]
24. Zhang, J.; Peng, W.; Chen, Z.; Chen, H.; Han, L. Effect of cerium doping in the TiO_2 photoanode on the electron transport of dye-sensitized solar cells. *J. Phys. Chem. C* **2012**, *116*, 19182–19190. [CrossRef]
25. Kazmi, S.A.; Hameed, S.; Ahmed, A.S.; Arshad, M.; Azam, A. Electrical and optical properties of graphene-TiO_2 nanocomposite and its applications in dye sensitized solar cells (DSSC). *J. Alloys Compd.* **2017**, *691*, 659–665. [CrossRef]

26. Mehmood, U.; Ahmad, S.H.A.; Khan, A.U.H.; Qaiser, A.A. Co-sensitization of graphene/TiO_2 nanocomposite thin films with ruthenizer and metal free organic photosensitizers for improving the power conversion efficiency of dye-sensitized solar cells (DSSCs). *Sol. Energy* **2018**, *170*, 47–55. [CrossRef]
27. Xu, H.; Wu, X.; Li, X.; Luo, C.; Liang, F.; Orignac, E.; Zhang, J.; Chu, J. Properties of graphene-metal contacts probed by Raman spectroscopy. *Carbon* **2018**, *127*, 491–497. [CrossRef]
28. Imbrogno, A.; Pandiyan, R.; Macario, A.; Bonanno, A.; El Khakani, M.A. Optimizing dye adsorption in graphene–TiO_2 photoanodes for the enhancement of photoconversion efficiency of DSSC devices. *IEEE J. Photovolt.* **2019**, *9*, 1240–1248. [CrossRef]
29. Zulkapli, M.F.; Rashid, N.M.; Sokri, M.N.M.; Nasri, N. Study on optical properties of graphene-TiO_2 nanocomposite as photoanodes layer in dye sensitized solar cell (DSSC). *Environ. Ecosyst. Sci.* **2018**, *2*, 39–41. [CrossRef]